

Optically tuned dielectric characteristics of $SrTiO_3$/Si thin film in the terahertz range

Bin Zou(邹斌), Qing-Qing Li(李晴晴), Yu-Ping Yang(杨玉平), and Hai-Zhong Guo(郭海中)

Citation: Chin. Phys. B, 2021, 30 (**10**): 107802. DOI: 10.1088/1674-1056/ac04a7
Journal homepage: http://cpb.iphy.ac.cn; http://iopscience.iop.org/cpb

What follows is a list of articles you may be interested in

Temperature dependent terahertz giant anisotropy and cycloidal spin wave modes in $BiFeO_3$ single crystal

Fan Liu(刘凡), Zuanming Jin(金钻明), Xiumei Liu(刘秀梅), Yuqing Fang(方雨青), Jiajia Guo(国家嘉), Yan Peng(彭滟), Zhenxiang Cheng(程振祥), Guohong Ma(马国宏), Yiming Zhu(朱亦鸣)
Chin. Phys. B, 2020, 29 (**7**): 077804. DOI: 10.1088/1674-1056/ab8dae

Variable angle spectroscopic ellipsometry and its applications in determining optical constants of chalcogenide glasses in infrared

Ning-Ning Wei(韦宁宁), Zhen Yang(杨振), Hong-Bo Pan(潘宏波), Fan Zhang(张凡), Yong-Xing Liu(刘永兴), Rong-Ping Wang(王荣平), Xiang Shen(沈祥), Shi-Xun Dai(戴世勋), Qiu-Hua Nie(聂秋华)
Chin. Phys. B, 2018, 27 (**6**): 067802. DOI: 10.1088/1674-1056/27/6/067802

Optically induced abnormal terahertz absorption in black silicon

Dong-Wei Zhai(翟东为), Hai-Ling Liu(刘海玲), Xxx Sedao, Yu-Ping Yang(杨玉平)
Chin. Phys. B, 2018, 27 (**2**): 027802. DOI: 10.1088/1674-1056/27/2/027802

Terahertz time-domain spectroscopy of a simulated pore structure to probe particle size and porosity of porous rock

Dong Chen, Bao Ri-Ma, Zhao Kun, Xu Chang-Hong, Jin Wu-Jun, Zhong Shou-Xian
Chin. Phys. B, 2014, 23 (**12**): 127802. DOI: 10.1088/1674-1056/23/12/127802

Pressure-dependent terahertz optical characterization of heptafluoropropane

Leng Wen-Xiu, Ge Li-Na, Xu Shan-Sen, Zhan Hong-Lei, Zhao Kun
Chin. Phys. B, 2014, 23 (**10**): 107804. DOI: 10.1088/1674-1056/23/10/107804

Optically tuned dielectric characteristics of $SrTiO_3$/Si thin film in the terahertz range*

Bin Zou(邹斌)[1,3], Qing-Qing Li(李晴晴)[1,2], Yu-Ping Yang(杨玉平)[1,3,†], and Hai-Zhong Guo(郭海中)[2,4,‡]

[1] School of Science, Minzu University of China, Beijing 100081, China
[2] School of Physics and Microelectronics, Zhengzhou University, Zhengzhou 450052, China
[3] Optoelectronics Research Center, Minzu University of China, Beijing 100081, China
[4] Collaborative Innovation Center of Light Manipulations and Applications, Shandong Normal University, Jinan 250358, China

(Received 19 March 2021; revised manuscript received 4 May 2021; accepted manuscript online 25 May 2021)

Active control of the optical parameters in strontium titanate ($SrTiO_3$, STO) thin films is highly desirable for tunable terahertz (THz) integrated devices such as filters, phase modulators, and electro-optical devices. In this work, optically tuned dielectric parameters of a STO thin film epitaxially grown on a silicon wafer were characterized in the THz region with an 800 nm laser pump-THz detection system. The refractive index, extinction coefficient, and complex dielectric constant of the STO thin film were calculated using thin-film parameter extraction. Owing to carrier transportation and soft-mode oscillation, the above optical parameters changed notably with the pump power of the external laser. This study is of great significance for rapid and non-contact THz phase-modulation technology and may serve as a powerful tool to tune the dielectric properties of the STO thin films.

Keywords: terahertz spectroscopy, optical constants, STO/Si film

PACS: 78.47.jh, 78.20.Ci, 78.66.–W **DOI:** 10.1088/1674-1056/ac04a7

1. Introduction

Terahertz (THz) tunable devices have attracted considerable attention for their efficient manipulation of the local phase, amplitude, and polarization on a subwavelength scale.[1,2] In the past decade, great advancements have been made in modulating THz waves by controlling the electrical, magnetic, thermal, and mechanical characteristics of artificial metasurfaces and new materials, including semiconductors (silicon, sapphire, GaAs, etc.), superconductors (YBCO, NbN, etc.), two-dimensional materials (graphene, MoS_2, black phosphorus, etc.), and phase transition materials (VO_2, etc.).[3–15] However, applications of these materials and devices have been limited in part because their tunable physical parameters are mainly focused on electric conductivity and amplitude response using complex preparation processes (doping, vacancy, etc.) and modulation means (light, electricity, heat, etc.). There is a relative deficiency of studies on dielectric properties such as refractive index, dielectric constant, and phase modulation. Therefore, it is of great significance to find suitable materials with controllable dielectric properties, which are essential parameters for understanding the tunable properties of these materials for THz wave modulation technology.

Strontium titanate ($SrTiO_3$, STO) is a perovskite-type oxide with unique ferroelectric and dielectric properties, including a high dielectric constant, low dielectric loss, and good thermal stability. In addition, the relative permittivity (ε_r) of STO can be determined fundamentally by its strong ferroelectric soft mode.[16,17] Thus, the dielectric properties of STO can be tuned effectively through soft-mode dynamics by modulating the temperature or external direct-current (or low frequency) electric field.[18,19] Thin ferroelectric films are especially attractive for tunable applications because of their lower tuning bias, higher modulation speed, and potential for monolithic integration. As a result, STO thin film is very promising for the development of fast-acting THz integrated devices such as tunable filters, phase modulators, and electro-optical devices.[20,21]

In 2006, Kužel *et al.*[22] demonstrated an electric-field induced variation of the permittivity of the STO thin film from the MHz up to THz frequency range. Komandin *et al.*[16,17] investigated the dielectric constant of (Ba, Sr)TiO_3 film in the range of 8–1000 cm^{-1}. The results indicate that the dielectric constant of the $Ba_{0.7}Sr_{0.3}TiO_3$ film in the THz band is as high as 400–600 and changes with the thickness of the film. In addition, the temperature tunability of the ferroelectric soft mode of the STO film and the STO/$DyScO_3$ heterostruture was also investigated. Furthermore, a group of all-dielectric metamaterials composed of STO rods was designed by Yahiaoui *et al.*[20,21] and realized negative permeability in multiple fre-

*Project supported by the National Natural Science Foundation of China (Grant No. 62075248), the National Key R&D Program of China (Grant Nos. 2017YFB0405400 and 2020YFB2009300), and the Program for the Innovation Team of Science and Technology in University of Henan, China (Grant No. 20IRTSTHN014).

†Corresponding author. E-mail: ypyang@muc.edu.cn
‡Corresponding author. E-mail: hguo@zzu.edu.cn

© 2021 Chinese Physical Society and IOP Publishing Ltd

quency bands, which can be adjusted continuously by changing the temperature. Qi *et al.*[23] also designed a split-ring-resonator (SRR) metamaterial based on the $Ba_{0.7}Sr_{0.3}TiO_3$ films at different temperatures, and obtained the dielectric constant of (Ba, Sr)TiO_3 films in the temperature range of 0–100 °C. Wu *et al.*[24–26] reported the electromagnetic response of bulk STO:Fe and STO single crystals in an external optical field, showing some unique characteristics of short response time, large modulation depth, and reusability.

Considering the above works, most observations have been carried out by varying the temperature or the electric-field in bulk STO crystals. The thin STO film offers several advantages over bulk materials, such as lower driving voltage, higher modulation speed, and better potential applications for monolithic integration. The dielectric tunability of the STO thin films under an optical field, however, has rarely been reported as it is difficult to identify the dielectric properties of ferroelectric thin films and they exhibit process-dependent properties.[27–30] Moreover, considerably fewer studies have focused on the THz regime. In this work, we investigated the active control of optical parameters of the STO thin film grown on silicon substrate (STO/Si) under the irradiation of an 800 nm laser. The variation of complex refractive index and dielectric constant at THz frequencies was investigated and discussed. We aim to find a suitable material with controllable dielectric properties in the THz region.

2. Experimental methods

Epitaxial crystalline perovskite oxide thin films on silicon (Si) simply by virtue of their high dielectric constants, could fundamentally change the scaling laws for silicon-based transistor technology.[31–33] Here, the STO thin-film sample was grown on a (100) silicon substrate by laser molecular beam epitaxy using a XeCl excimer laser (Lambda LEXTRA 200, $\lambda = 308$ nm, 2 Hz, 1.5 J/cm^2). A Si (100) substrate (p-type, 12.95 Ω·cm) was carefully cleaned and was dipped into HF (4%) solution for 30–40 second to remove the amorphous SiO_2 layer from the silicon surface, leaving a hydrogen-terminated surface. Subsequently, the Si substrate was immediately moved into the epitaxial chamber. The initial deposition of about two atomic-layers of SrO film was under the base pressure of 5×10^{-6} Pa at the substrate temperature of 300 °C to prevent the formation of the SiO_2 interface layer. After that, the substrate temperature was raised to 620 °C. When the so treated SrO surface showed a sharp streaky RHEED pattern, the oxygen pressure was raised to 2×10^{-4} Pa. Then, the $SrTiO_3$ thin film with a thickness of 15 nm was deposited and *in situ* annealed for 20 minutes. X-ray diffraction showed that the STO film is single-crystal thin film without any impurity phases. The descriptions of the growth and the measurements of the structure and crystalline qualities have been reported in our previous work.[33]

We characterized the dielectric tunability of the STO thin film using a terahertz time-domain spectroscopy (THz-TDS) system with a pair of photoconductive antennas for both generation and detection of THz waves, as shown in Fig. 1. A mode-locked Ti:sapphire femtosecond laser with a central wavelength of 800 nm, pulse duration of 100 fs, and repetition rate of 80 MHz was used as the optical source. The THz radiation generated form the THz emitter was collimated by a high-resistivity Si lens and a parabolic mirror (PM1). The STO/Si sample was placed at the midpoint of the $4f$ THz-TDS system. A continuum solid-state laser with a wavelength of 800 nm was focused to irradiate on the STO surface, with the laser power (P) varied from 0 to 6 W. The diameters of the spot sizes of the THz beam and continuous-wave (CW) laser were approximately 0.8 cm and 1.5 cm, respectively. Detailed information of the system and data process has been reported in previous works.[8,34]

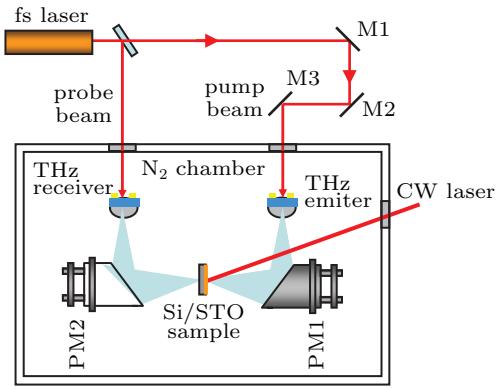


Fig. 1. Schematic diagram of the measurement system.

3. Results and discussion

The temporal THz waveforms that passed through the blank Si substrate and STO/Si sample are shown in Fig. 2(a) with the laser turned off. Compared with the bare substrate (E_r), the transmitted THz pulse through the STO/Si sample (E_s) shows a slight decrease in signal amplitude and a short shifting delay time of 0.06 ps, indicating that the 15-nm-thick STO film has a very high dielectric constant and refractive index. Figure 2(b) illustrates the evolution of the THz wave when passing through the blank silicon substrate with the pump power increasing from 0 to 6 W. It can be found that the THz time-domain signal decreases gradually as the intensity of the laser beam increases, but the shape and position of the main peak remain almost unchanged. As can be seen in Fig. 2(c), the variation of the THz pulse transmitted through the STO/Si sample with different pump powers is similar to that in the silicon substrate. A monotonous decrease in amplitude from 0.79 to 0.34 was also observed under the laser irradi-

ation, while the time delay increased with increasing the laser power. The peak of the transmitted THz signal at $P = 6$ W drifts by approximately 0.10 ps compared with that at $P = 0$ W.

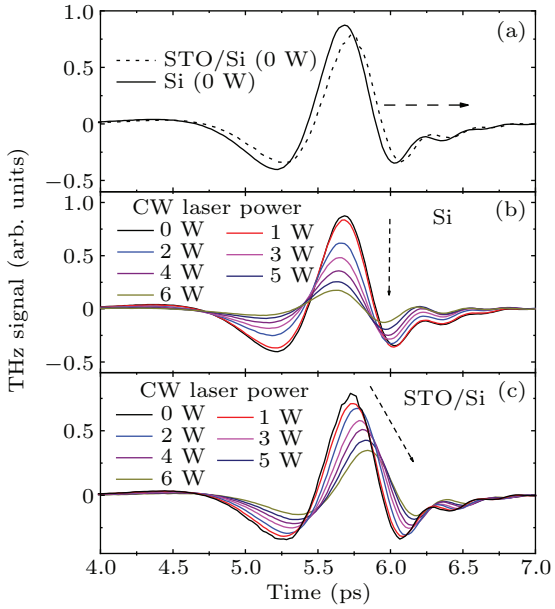


Fig. 2. THz waveforms of (a) samples without optical pump, (b) bare silicon substrate, and (c) the STO/Si sample with different laser powers.

To extract the optical parameters of the thin STO film, the THz pulse passing through the blank Si substrate is used as a reference ($E_r(t)$), and the transmitted THz signal of the STO/Si sample is used as a sample ($E_s(t)$). The ratio between the Fourier transformations of $E_r(t)$ and $E_s(t)$ is $t(\omega) = E_s(\omega)/E_r(\omega) = \rho\, e^{i\delta}$. For the ultrathin STO film in this work, the complex dielectric constant of the STO film $\tilde{\varepsilon}(\omega) = \varepsilon_r(\omega) + i\varepsilon_i(\omega)$ can be represented by the following expressions:[35]

$$\varepsilon_r(\omega) = \frac{c}{\omega d}(n_1 + n_3)\rho \sin\delta - n_1 n_3 + n_1 + n_3, \quad (1)$$

$$\varepsilon_i(\omega) = \frac{(1 - \rho\cos\delta)c}{\omega d}(n_1 + n_3). \quad (2)$$

Here, n_1 ($n_1 = 1$) and n_3 ($n_3 = 3.42$) are the refractive indices of air and silicon, respectively; $d = 15$ nm is the film thickness; and c is the speed of light in vacuum. The complex refractive index of the STO thin film is $\tilde{n}(\omega) = n(\omega) + i\kappa(\omega)$, which can be deduced by

$$n = \frac{1}{\sqrt{2}}[\varepsilon_r + \sqrt{\varepsilon_r^2 + \varepsilon_i^2}]^{1/2}, \quad (3)$$

$$\kappa = \frac{1}{\sqrt{2}}[-\varepsilon_r + \sqrt{\varepsilon_r^2 + \varepsilon_i^2}]^{1/2}, \quad (4)$$

where n and κ are the real refractive index and extinction coefficient of the STO film, respectively. The complex refractive index and permittivity of the thin STO film calculated by Eqs. (1)–(4) are shown in Figs. 3–5.

Figure 3 shows the frequency-dependent refractive index and extinction coefficient of the STO film under different powers. It is clear from Fig. 3(a) that the average refractive index of the STO film without laser pumping is aproximately 61 in the range of 0.5–2.5 THz. In addition, the refractive index of the STO film at 1.5 THz increases from 61 to 133 with increasing laser power from 0 to 6 W. There is a strong linear relationship between the refractive index and the laser power, as shown in Fig. 3(b). The extinction coefficient spectra, depicted in Fig. 3(c), reflect the absorption characteristics of the sample. Under the lower laser irradiation ($P < 2$ W), the extinction coefficient decreases with increasing frequency, and vice versa with the laser power higher than 2 W. In addition, the extinction coefficient increases with increasing the laser power at frequencies above 1.5 THz, and vice versa at frequencies below 1.5 THz. Thus, the relationship between the laser power and the extinction coefficient is not linear. Based on these results, more than one absorption mechanisms account for the absorption of THz wave, and these mechanisms are strongly influenced by the exciting laser. Overall, a derivative-like shape of the extinction coefficient spectra data in the range of 1.0–2.0 THz can be well agreed with the linear function, and the fitting slope of the extinction coefficient curve increases with increasing the exciting intensity. To gain further insight into the response, the fitting slope of the rising extinction coefficient in the range of 1.0–2.0 THz is plotted against the laser power and a linear relationship is found between them, as displayed in Fig. 3(d).

As can be seen in Figs. 4(a) and 5(a), the real and imaginary parts of the dielectric constant of the STO film in the range of 0.5–2.5 THz under different powers are similar to those in Figs. 3(a) and 3(c), respectively. The real part of the complex permittivity is caused by various types of displacement polarization in the material, and represents the energy storage term of the material. The imaginary part of the complex permittivity represents the loss term of the material caused by various types of relaxation polarization. It can be found that the real part of the dielectric constant of the STO film changes notably in the range of 4000–50000, and decreases monotonically with increasing frequency. In addition, the real part increases with increasing pump power, which indicates that the displacement polarization in the STO film increases under the excitation of the laser beam. Simultaneously, due to an increase in the dispersion and absorption effect, the rate of decrease of ε_r with frequency also increases significantly, thus, ε_r decreases with increasing pump power at high frequency range. Figure 4(b) shows the fitting slope of ε_r in the range of 1.0–2.0 THz. In the case of weak absorption (κ is very small), $|\Delta\varepsilon_r| \propto n$ due to $\varepsilon_r = n^2 - \kappa^2$. Thus, the change of $|\Delta\varepsilon_r|$ with power should be consistent with the change of refractive index n with power (as shown in Fig. 3(b)). As can be seen in Fig. 4(b), however, the relationship between the laser power and the slope of ε_r is not linear but shows an exponential rise, indicating that the STO film has a strong absorption under the laser irradiation.

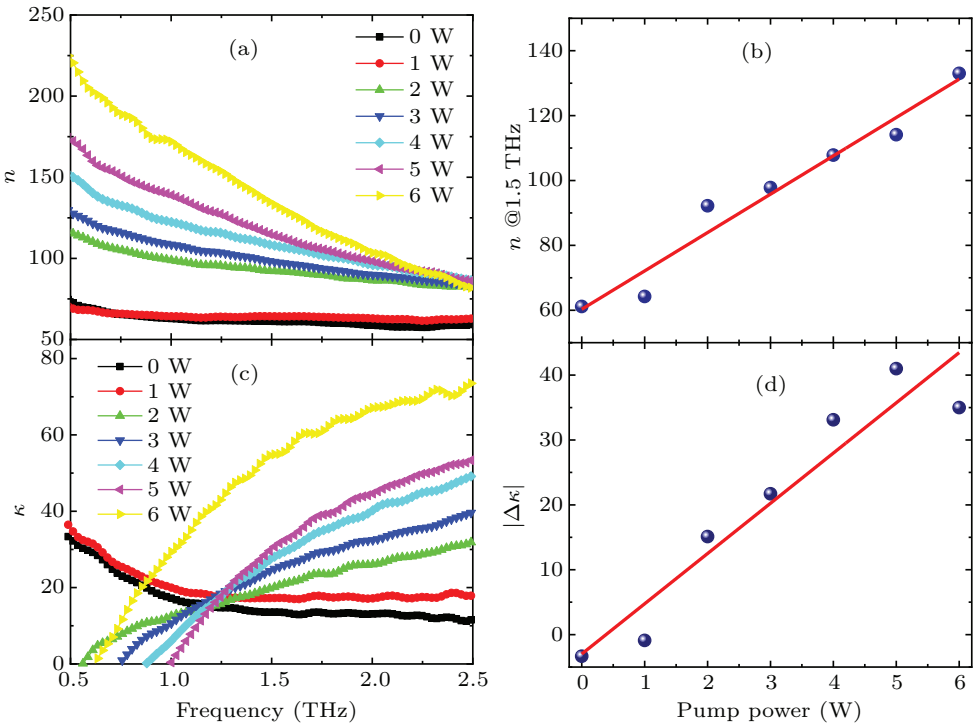


Fig. 3. (a) Frequency-dependent refractive index under 800 nm laser irradiation with different laser powers; and (b) variation of refractive index at 1.5 THz vs. laser power; (c) frequency-dependent extinction coefficient under 800 nm laser irradiation with different laser powers; and (d) slope of extinction coefficient in the range of 1.0–2.0 THz vs. laser power.

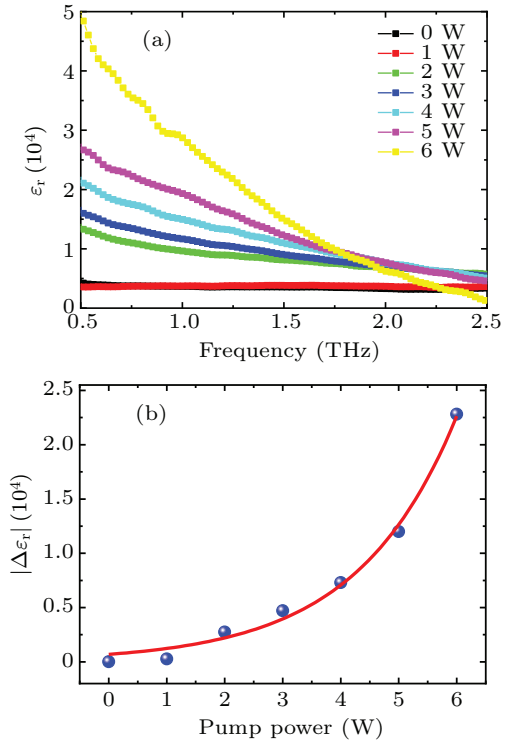


Fig. 4. (a) Real part of the dielectric constant and (b) its slope in the range of 1.0–2.0 THz under different laser powers.

Because the energy of the 800 nm laser is higher than the band gap of silicon, a large number of photogenerated carriers are generated in the silicon substrate and diffuse to the STO thin film and the other interface of the silicon wafer. Consequently, the conductivity is enhanced by the movement of the photogenerated carriers and a surface field is formed due to the different mobilities of electrons and holes. On the other hand, the conductivity and surface electric field further affect the soft-mode resonance. Thus, the spectroscopic data of the STO film in the range of 0.5–2.5 THz have relied on the diffusive behavior of the photogenerated carriers and oscillatory motion of the soft-mode resonance. The Drude model is ordinarily suitable for two-dimensional-free electron gas with complete momentum randomization following elastic scattering events. In addition, the Lorentz model is generally appropriate for resonance polarization in dielectrics with the damped harmonic oscillator. The frequency-dependent, complex permittivity, $\tilde{\varepsilon}(\omega) = \varepsilon_r(\omega) + i\varepsilon_i(\omega)$, provides a fundamental description of the STO film, which ban be described by a sum of Drude formula and single resonance Lorentz function[36]

$$\tilde{\varepsilon}(\omega) = \varepsilon_\infty + \frac{S \cdot \omega_p^2}{\omega_s^2 - \omega^2 - i\gamma\omega} - \frac{\omega_p^2}{\omega^2 + i\Gamma_p\omega}, \tag{5}$$

where ε_∞ is the high-frequency dielectric constant; the second term represents the Lorentz oscillation, which describes the damped harmonic oscillation of the bonded charge; and the third term is described as the Drude oscillation, which represents the contribution of nonlocalized conduction of the photogenerated carriers. ω_p and Γ_p are the plasma frequency and charge relaxation rate, respectively. ω_s, γ, and S represent the angular frequency, peak width, and oscillation intensity of the soft mode oscillation (TO1 phonon resonance), respectively. The imaginary part of ε_i can be expressed as

$$\varepsilon_i(\omega) = \frac{S \cdot \omega_p^2 \cdot \gamma\omega}{(\omega_s^2 - \omega^2)^2 + \gamma^2\omega^2} + \frac{\omega_p^2\Gamma_p}{\omega^3 + \Gamma_p^2\omega}. \tag{6}$$

The solid line in Fig. 5(a) is the calculated imaginary part of the dielectric constant according to Eq. (6) under different pump powers. It can be seen that the theoretical curves are in good agreement with the experimental results. The fitted values of the soft-mode frequency ($\omega_s/2\pi$) are listed in Table 1. Figure 5(b) shows that the soft-mode frequency decreases linearly with increasing laser power.

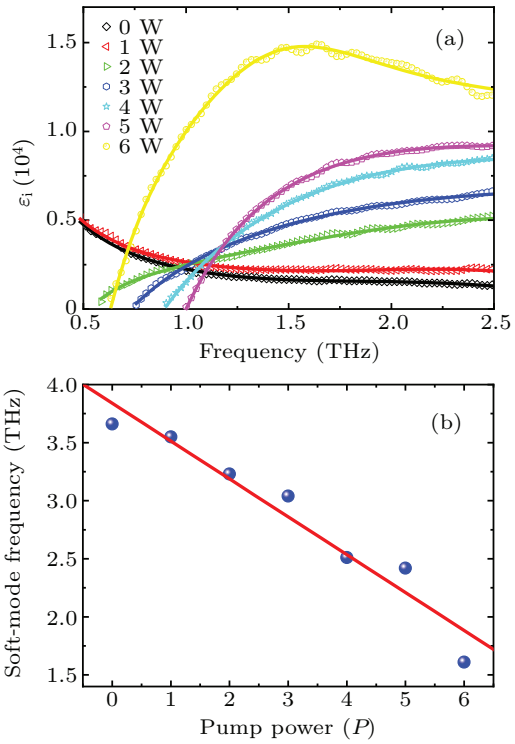


Fig. 5. (a) Imaginary part of the dielectric constant under different laser powers; (b) dependence of the fitted value of $\omega_s/2\pi$ on the laser power P.

Table 1. Fitted values of the soft mode frequency under different powers.

Power (W)	0	1	2	3	4	5	6
$\omega_s/2\pi$ (THz)	3.66	3.55	3.23	3.05	2.51	2.42	1.62

The soft-mode frequency of the STO bulk material was reported to be in the range of 2.7–3.0 THz and determined by the thickness, interface stress, temperature, electric field, and other factors.[20–28,30–33] When an 800 nm CW laser irradiates the sample, temperature variation is inevitably introduced. To further characterize the temperature-dependent optical parameters of the STO/Si sample, the THz time-domain waveforms were measured at different temperatures and illustrated in Fig. 6. It was found that the amplitudes of the THz signals changed slightly and the time delay remained almost unchanged as the temperature was varied from 20 °C to 55 °C. Therefore, we excluded the temperature influence on the modulation of the external light field.

However, the dielectric constants obtained here were higher than the values reported for $SrTiO_3$ films obtained by other techniques, considering about the same thickness.[17,19,22] The increased dielectric constant in the THz range is believed to be related to interfacial polarization of space charges. Photoexcitation with 800 nm light does only produce carriers in the silicon substrate, but not in the STO film due to the wider band gap. Because the photogenerated electrons and holes have different mobilities, diffusion voltage was caused on the front and back surfaces of the silicon substrate, known as Dember voltage, as shown in Fig. 7. The optical skin depth is on the order of the 10 μm thickness of silicon layer with 800 nm photoexcitation, and leads to the Dember electric field up to 10^4 V/cm.[37] In addition, the Dember electric field increases with increasing laser power, $E_{\text{Dember}} \propto I$, which may have induced an increase in displacement polarization and dielectric constant in the STO film. The change in dielectric constant directly led to a change in the refractive index. Generally, the shift of refractive index due to linear EO effect (Pockels effect) is given by $\Delta n \propto E_{\text{Dember}} \propto I$. Thus, the refractive index of the sample was changed and exhibited a linear dependence on the laser intensity. Also, the photovoltaic field can change some internal characteristics of STO film, such as the domain structure, coercive field, and so on, so as to further modulate the resonance frequency of the soft mode. However, the observed frequency softening of the soft-mode resonance in this work is quite different from the hardening of TO1 mode in KTO crystal under external light field.[38] Further work should be conducted on electrical monitoring with a voltage-varying system, experimentally finding a special correlation between the soft-mode frequency and electric field.

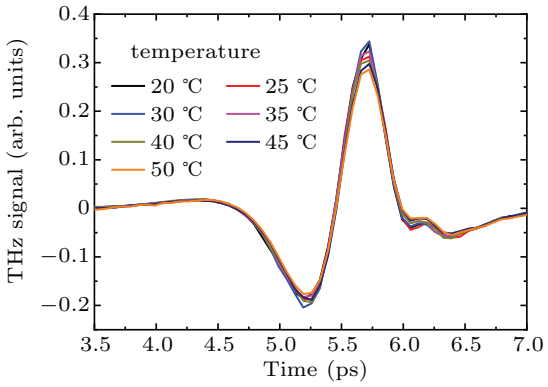


Fig. 6. THz signals under different temperatures.

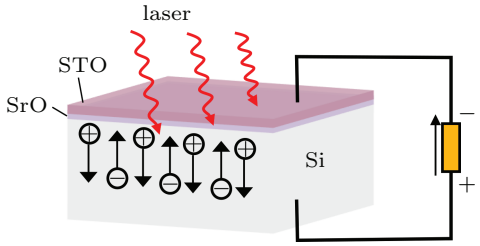


Fig. 7. Schematic diagram of the Dember electric field formed by carrier transportation.

4. Conclusions

The dielectric response of a 15-nm thick $SrTiO_3$ thin film grown on a silicon substrate in the THz range was measured using an 800 nm CW laser pump-THz detection system. With the laser on, both the number of photogenerated carriers and the Dember electric field were increased with laser power, giving rise to stronger absorption and displacement polarization. It was observed that the refractive index, extinction coefficient, and real and imaginary parts of the dielectric constant varied notably with the laser power. Moreover, the resonant frequency of the soft mode was linearly related to the laser power. The results presented here are of great significance for rapid and non-contact THz phase-modulation technology, and may serve as a powerful tool to tune the dielectric properties of STO thin films.

Appendix A: Thin-film parameter extraction

The refractive index, dielectric constant, and other optical parameters of the STO film can be extracted by comparing the temporal THz waveforms with or without the STO thin film on silicon substrate. The schematic diagram of the THz transmission field is shown in Fig. A1, where n_1 is the refractive index of air, $\tilde{n} = n + \mathrm{i}\kappa$ is the complex refractive index of the film, and n_3 is the refractive index of the silicon substrate. Here, $n_1 = 1$, $n_3 = 3.42$, n is the real refractive index, and κ is the extinction coefficient, $\tilde{n}^2 = (n + \mathrm{i}\kappa)^2 = \varepsilon_\mathrm{r} + \mathrm{i}\varepsilon_\mathrm{i}$.

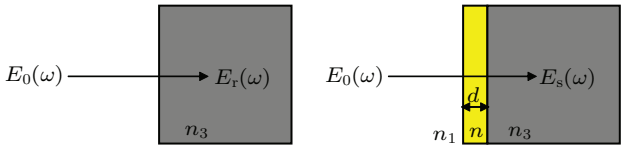


Fig. A1. Schematic diagram of film parameter extraction.

In Fig. A1, $E_0(\omega)$ is the incident THz electric field, $E_\mathrm{r}(\omega)$ is the transmitted THz field through the bare substrate, $E_\mathrm{s}(\omega)$ is the transmitted THz field through the STO/Si sample, and d is the thickness of the film

$$E_\mathrm{r}(\omega) = t_{13}\mathrm{E}_0(\omega)\mathrm{e}^{\mathrm{i}\omega d/c}, \tag{A1}$$

$$E_\mathrm{s}(\omega) = \frac{t_{23}t_{12}\mathrm{e}^{\mathrm{i}\omega nd/c}}{1 - r_{21}r_{23}\mathrm{e}^{\mathrm{i}2nd\omega/c}}E_0(\omega), \tag{A2}$$

in which c is the speed of light and $\omega = 2\pi f$ is the angular frequency. According to the Fresnel formula, the reflection and transmission coefficients of the THz wave at the three interfaces are respectively obtained as follows: $r_{21} = (n - n_1)/(n + n_1)$, $r_{23} = (n - n_3)/(n + n_3)$, $t_{13} = 2n_1/(n_1 + n_3)$, $t_{23} = 2n/(n + n_3)$, and $t_{12} = 2n/(n_1 + n)$; then

$$\frac{E_\mathrm{s}(\omega)}{E_\mathrm{r}(\omega)} = \frac{t_{23}t_{12}\mathrm{e}^{\mathrm{i}\omega(n-1)d/c}}{t_{13}(1 - r_{21}r_{23}\,\mathrm{e}^{\mathrm{i}2\omega nd/\mathrm{c}})}, \tag{A3}$$

in which $\mathrm{e}^{\mathrm{i}\omega(n-1)d/c} \sim 1 + \mathrm{i}\omega(n-1)d/c$ because $\omega(n-1)d/c \ll 1$, and $\mathrm{e}^{\mathrm{i}2\omega nd/c} \sim 1 + \mathrm{i}2\omega nd/c$ because $d \ll 1$ and $2\omega nd/c \ll 1$; then

$$\frac{t_{12}t_{23}}{t_{13}}\mathrm{e}^{\mathrm{i}\omega(n-1)d/c} = \frac{2n(n_1+n_3)}{(n_1+\mathrm{n})(n+n_3)}\left[1 + \mathrm{i}\omega(n-1)d/c\right], \tag{A4}$$

$$1 - r_{21}r_{23}\,\mathrm{e}^{\mathrm{i}2\omega nd/c} = \frac{2n(n_1+n_3) - (n-n_1)(n-n_3)2\mathrm{i}\omega nd/c}{(n+n_1)(n+n_3)}, \tag{A5}$$

$$\frac{E_\mathrm{s}}{E_\mathrm{r}} = 1 + \frac{\mathrm{i}2n(n+n_3)\omega(n-1)d/c + (n-n_1)(n-n_3)2\mathrm{i}\omega nd/c}{2n(n_1+n_3) - (n-n_1)(n-n_3)2\mathrm{i}\omega nd/c}. \tag{A6}$$

As $\omega d/c \ll 1$, Eq. (A6) can be reduced to

$$\frac{E_\mathrm{s}}{E_\mathrm{r}} = 1 + \frac{\mathrm{i}\omega d}{c(n_1+n_3)}\left[-n_1 + n_1n_3 + (n + \mathrm{i}\kappa)^2 - n_3\right]. \tag{A7}$$

If Eq. (A7) is simplified to $\rho\,\mathrm{e}^{\mathrm{i}\delta}$, then

$$\frac{E_\mathrm{s}}{E_\mathrm{r}} = 1 + \frac{\mathrm{i}\omega d}{c(n_1+n_3)}\left[-n_1 + n_1n_3 + (\varepsilon_\mathrm{r} + \mathrm{i}\varepsilon_\mathrm{i}) - n_3\right] = \rho\,\mathrm{e}^{\mathrm{i}\delta}, \tag{A8}$$

$$\rho\cos\delta = 1 - \frac{\omega d}{c(n_1+n_3)}\varepsilon_\mathrm{i}, \tag{A9}$$

$$\rho\sin\delta = \frac{\omega d}{c(n_1+n_3)}(-n_1 + n_1n_3 + \varepsilon_\mathrm{r} - n_3). \tag{A10}$$

For a thin film, i.e., $|n\omega d/c| \ll 1$, the dielectric response $\tilde{\varepsilon} = \varepsilon_\mathrm{r} + \mathrm{i}\varepsilon_\mathrm{i}$ can be represented by the following expressions:[35]

$$\varepsilon_\mathrm{r}(\omega) = \frac{c}{\omega d}(n_1+n_3)\rho\sin\delta - n_1n_3 + n_1 + n_3, \tag{A11}$$

$$\varepsilon_\mathrm{i}(\omega) = \frac{c}{\omega d}(n_1+n_3)(1 - \rho\cos\delta). \tag{A12}$$

The complex refractive index of the STO thin film $\tilde{n} = n + \mathrm{i}\kappa$ can be deduced by

$$n = \frac{1}{\sqrt{2}}\left[\varepsilon_\mathrm{r} + \sqrt{\varepsilon_\mathrm{r}^2 + \varepsilon_\mathrm{i}^2}\right]^{1/2}, \tag{A13}$$

$$\kappa = \frac{1}{\sqrt{2}}\left[-\varepsilon_\mathrm{r} + \sqrt{\varepsilon_\mathrm{r}^2 + \varepsilon_\mathrm{i}^2}\right]^{1/2}. \tag{A14}$$

References

[1] Zhang X, Xu Q, Xia L, Li Y, Gu J, Tian Z, Ouyang C, Han J and Zhang W 2020 *Adv. Photon.* **2** 014001

[2] Ma Q and Cui T 2020 *Photonix* **1** 1

[3] Chen H T, Padilla W J, Zide J M O, Gossard A C, Taylor A J and Averitt R D 2006 *Nature* **444** 597

[4] Gu J, Singh R, Liu X, Zhang X, Ma Y, Zhang S, Maier S A, Tian Z, Azad A K, Chen H T, Taylor A J, Han J and Zhang W 2012 *Nat. Commun.* **3** 1151

[5] Lee S H, Choi M, Kim T T, Lee S, Liu M, Yin X, Choi H K, Lee S S, Choi C G, Choi S Y, Zhang X and Min B 2012 *Nat. Mater.* **11** 936

[6] Li L, Yu Y, Ye G, Ge Q, Ou X, Wu H, Feng D, Xia H and Zhang Y 2014 *Nat. Nanotech.* **9** 372

[7] Zhao T, Zhong R B, Hu M, Chen X X, Zhang P, Gong S and Liu S G 2015 *Chin. Phys. B* **24** 094102

[8] Cao Y, Gan S, Geng Z, Liu J, Yang Y, Bao Q and Chen H 2016 *Sci. Rep.* **6** 22899

[9] Chen H, Wen X, Zhang J, Wu T, Gong Y, Zhang X, Yuan J, Yi C, Lou J, Ajayan P M, Zhuang W, Zhang G and Zheng J 2016 *Nat. Commun.* **7** 12512

[10] Zhong S, Lu Y, Li C, Xu H, Shi F and Chen Y 2017 *Sci. Rep.* **7** 41788

[11] Cong L, Srivastava Y K, Zhang H, Zhang X, Han J and Singh R 2018 *Light: Science & Applications* **7** 28

[12] Shen Z X, Zhou S H, Ge S J, Hu W and Lu Y Q 2019 *Appl. Phys. Lett.* **114** 041106

[13] Wu J, Shen Z, Ge S, Chen B, Shen Z, Wang T, Zhang C, Hu W, Fan K, Padilla W, Lu Y, Jin B, Chen J and Wu P 2020 *Appl. Phys. Lett.* **116** 131104

[14] Li Q, Gupta M, Zhang X, Zhang S, Chen T, Singh R, Han J and Zhang W 2020 *Adv. Mater. Technol.* **5** 1900840

[15] Chen S C, Yuan H K, Zhai Z, Du L H, Zhong S C, Zhu H F, Shi Q, Huang W X, Li Z R and Zhu L 2020 *Opt. Lett.* **45** 236

[16] Komandin G A, Volkov A A, Spektor I E, Vorotilov K A and Mukhortov V M 2009 *Phys. Solid State* **51** 1351

[17] Komandin G A, Mukhortov V M, Porodnikov O E and Spektor I E 2013 *Phys. Solid State* **55** 288

[18] Liang Y, Li W, Zhang S, Lin C, Li C, Yao Y, Li Y, Yang H and Guo J 2015 *Sci. Rep.* **5** 10634

[19] Zhang Y, Yan Q, Yang F, Xu Y and Liu L 2016 *Ceramics International* **42** 12672

[20] Yahiaoui R, Němec H, Kužel P, Kadlec F, Kadlec C and Mounaix P 2011 *Appl. Phys. A* **103** 689

[21] Yahiaoui R, Němec H, Kužel P, Kadlec F, Kadlec C and Mounaix P 2009 *Opt. Lett.* **34** 3541

[22] Kužel P, Kadlec F, Němec H, Ott R, Hollmann E and Klein N 2006 *Appl. Phys. Lett.* **88** 102901

[23] Qi P, Fan Y, Li H, Zhang Q and Zhai J 2012 *J. Am. Ceram. Soc.* **95** 1167

[24] Wu L, Jiang L, Sheng Q, Ding X and Yao J 2013 *Opt. Lett.* **38** 2581

[25] Wu L, Jiang L, Cai Y, Ding X and Yao J 2014 *Chin. Phys. B* **23** 034212

[26] Wu L, Du T, Xu N N, Ding C F, Li H, Sheng Q, Liu M, Yao J Q, Wang Z Y, Lou X J and Zhang W 2016 *Small* **12** 2610

[27] Kinjo R, Kawayama I, Murakami H and Tonouchi M 2013 *Advances in Materials Physics and Chemistry* **3** 58

[28] Pontes F M, Lee E J H, Leite E R, Longo E and Varela J A 2000 *Journal of Materials Science* **35** 4783

[29] Li S Z, Yang Y Q, Liu L, Liu W C and Wang S B 2008 *Physica B* **403** 2618

[30] Wang D Y, Wang J, Chan H L W and Choy C L 2007 *J. Appl. Phys.* **101** 043515

[31] McKee R A, Walker F J and Chisholm M F 1998 *Phys. Rev. Lett.* **81** 3014

[32] Warusawithana M P, Cen C, Sleasman C R, Woicik J C, Li Y, Kourkoutis L F, Klug J A, Li H, Ryan P, Wang L P, Bedzyk M, Muller D A, Chen L Q, Levy J and Schlom D G 2009 *Science* **324** 367

[33] Guo H, Huang Y, Jin K, Zhou Q, Lu H, Liu L, Zhou Y, Cheng B and Chen Z 2005 *Appl. Phys. Lett.* **86** 123502

[34] Zhai D W, Liu H L, Sedao X and Yang Y P 2018 *Chin. Phys. B* **27** 027802

[35] Tsai T R, Chen S J, Chang C F, Hsu S H, Lin T Y and Chi C C 2006 *Opt. Express* **14** 4898

[36] Yang Y, Feng S, Feng H, Pan X, Wang Y and Wang W 2011 *Acta Phys. Sin.* **60** 027802 (in Chinese)

[37] Aspnes D E and Studna A A 1983 *Phys. Rev. B* **27** 985

[38] Wu L, Li H, Jiang L, Ding C, Sheng Q and Yao J 2014 *Opt. Mat. Express* **4** 2595